A DYNAMIC MODEL FOR A MULTI-STAGE CO2 THERMAL COMPRESSOR HEAT PUMP APPLICATION

Ali Salame[a,b,c], Vincent Lemort[b], Pascal Dufour[c], Madiha Nadri[c]

[a]Boostheat Company, 41-47 Bd Marcel Sembat, 69200 Vénissieux, France

[b]Energy Systems Research Unit (B49), University of Liège, Sart-Tilman, Liège 4000, Belgium

[c] Univ Lyon, Université Claude Bernard Lyon 1, CNRS, LAGEPP UMR 5007, 43 boulevard du 11 novembre 1918, F-69100, VILLEURBANNE, France

Contact Email: alisalami0980@gmail.com

ABSTRACT

Thermally driven heat pumps primarily use thermal energy to drive a compression cycle. The thermal energy can be in the form of waste heat, combustion of natural gas, or solar energy, contributing to the demand for increased efficiency and reduced greenhouse gas emissions. A thermal compressor heat pump is one type in which the compressors are driven by heat as a primary source instead of electricity to deliver heat. Like any vapor compression cycle, a thermally driven heat pump cycle needs to be dynamically modeled for control and optimization purposes. A finite volume method is used to discretize the main heat exchangers (evaporator and gas cooler) into several control volumes, and mass and energy balance equations are applied to each. The connecting components, such as thermal compressors and high- and low-pressure valves, are statically modeled due to the difference in the rate of change compared to the heat exchangers. The important system performance indicators are validated at steady state and dynamically by varying key cycle inputs. This validated model serves as a reference for our thermal compressor heat pump application, which we aim to use for control law development and performance optimization.

1 INTRODUCTION

In 2023, 80% of our energy demand was met by burning oil, natural gas, and coal, according to IEA (2024). Switching entirely to renewables is a long and ongoing process, which we can meet halfway through more efficient usage of the dominant fossil fuels. Despite their great potential, electric heat pumps are still outcompeted by gas boilers due to several reasons beyond the scope of this work. That being said, and in an effort to bridge the gap between gas boilers and electric heat pumps, a Thermal Compressor Heat Pump (TCHP) is proposed, where heat is used to drive the heat pump cycle, benefiting from outdoor environmental conditions. The technology developed by Boostheat uses Stirling-type Thermal Compressors (TCs) instead of electric compressors. Another environmental advantage is the use of CO_2 as a refrigerant, which is increasingly encouraged today due to its environmentally friendly characteristics. The use of CO_2 adds more restrictions on cycle configurations due to its high critical pressure (73.8 bar) and low critical temperature (31.1 °C), which also motivates the use of more advanced control strategies to ensure optimal performance. For example, the performance of the CO_2 heat pump cycle is highly affected by the high pressure, as investigated by Neksa (2002) and Sarkar et al. (2006), where they showed that a higher coefficient of performance (COP) can be achieved when CO_2 is in its transcritical state. In such a state, the condenser acts as a gas cooler instead. A steady-state model for the CO_2 heat pump cycle was carried out by Yang et al. (2010), where they showed the influence of varying the high pressure on performance using both model simulations and experimental data, demonstrating good variation coherence despite not achieving high accuracy.
Dynamically, Pfafferott and Schmitz (2004) provided a Modelica-based transient model derived from mass and energy balance equations for a CO_2 refrigeration cycle, validated with experimental data.

Zheng et al. (2015) developed a model of a transcritical CO_2 ejector expansion refrigeration cycle capturing transient behavior under varying valve openings and ejector area ratios. Ko et al. (2020) used an object-oriented approach to model a CO_2 heat pump, validating it against experimental data for flow rate, heating capacity, and COP. Likewise, Diniz et al. (2021) modeled a solar-assisted heat pump for water heating based on mass, energy, and momentum balances, accurately simulating both steady and transient states.

More generally, the dynamic modeling methods of the Vapor Compression Cycle (VCC) can be categorized into two approaches: finite volume (FV), which spatially discretizes a heat exchanger into several control volumes where each carries thermal and physical information of the fluid, and moving boundary (MB), which is a lumped parameter model that divides a heat exchanger into regions according to fluid phases (liquid, two-phase, or vapor). An extensive literature review of the dynamic modeling approaches used for VCC was carried out by Rasmussen (2012). An attempt to compare both methods was made by Bendapudi et al. (2008) on centrifugal chillers, concluding that while the FV method resulted in higher computation time compared to MB, it was more robust. He et al. (1997) and Rasmussen (2005) introduced MB models for the condenser and evaporator, along with their linearization and some control laws. Although MB models consist of a limited number of ordinary differential equations, the order can still be reduced under the equilibrium assumption for certain variables, as shown by Peralez et al. (2017) and Erique et al. (2015).

In this work, we aim to introduce our TCHP cycle, which is a CO_2 multi-stage cycle with various heat exchangers. An MB system of equations depends on the state of CO_2 in the condenser/gas cooler, so we need to know or guess its state beforehand. Since it is preferable to operate CO_2 at high pressure values, we cannot know beforehand the state of CO_2 (whether two-phase or supercritical). To avoid having several hybrid models of the MB type (McKinley and Alleyne (2008)), we decided to use the FV method. Another reason for choosing the FV method is its robustness, particularly because the cycle consists of multiple stages and all the components' dynamics are interconnected. After introducing the cycle, we derived the models used for each component. Subsequently, the models of the gas cooler and evaporator were validated at a steady state. We then need to validate the transient responses, which are crucial for our control development. To the authors' best knowledge, this is the first attempt to dynamically model a multi-stage CO_2 TCHP using the Python programming language, with validation against real data.

2 Thermal Compressor Heat Pump Cycle

As illustrated in Figure 1, the cycle of a TCHP consists of three thermal compressors (TCs), three buffers, one gas cooler (GC), one evaporator (EVAP), an internal heat exchanger (IHX), flash tanks (FTs), two electronic expansion valves (EEVs), and a fume heat exchanger (FHX). At evaporation pressure, CO_2 enters the first-stage compressor and exits at a higher pressure. It is then cooled inside buffer 1 with a water flow and mixed with the vapor exiting the FT through a one-way valve before entering the second TC. The CO_2 then exits at a higher intermediary pressure and is cooled again inside the second buffer before entering the third TC. The buffers after each TC also act as dampers for the pressure waves resulting from compression. At its highest pressure level and high temperature, CO_2 rejects heat into the water entering the GC. It is then cooled again while passing inside one side of the IHX by the CO_2 exiting the EVAP, which passes through the other side. After exiting the IHX, the CO_2 refrigerant is expanded in a high-pressure valve (HPV), then enters a FT, where the CO_2 in its gaseous state is reinjected between the first and second TCs through a one-way valve, and the remaining liquid exits and expands in a low-pressure valve (LPV) before finally entering the EVAP.

For the water side (heating circuit), a smaller portion of the water flow goes to the buffers and the TCs, where it is subdivided again between the first two buffers and collected before consequently entering the coolers of the TCs. The largest part of the entering water goes to the gas cooler, where the two parts mix again before entering the FHX, where the resulting fumes from the combustion process are cooled. On the TCs side, the top parts of the first two TCs are connected to a burner fan, which is used to deliver the methane/air mixture into the top surfaces, i.e. heaters, where the gas mixture is burned to produce heat. The resulting fumes from both chambers are then directed to the top surface of the third TC before exiting into the FHX. The EVAP is heated by a mixture of monopropylene glycol-water (MPG), which

is cooled by a chiller to a certain temperature to mimic cold weather conditions. MPG is used because of its low freezing point, thus preventing frosting.

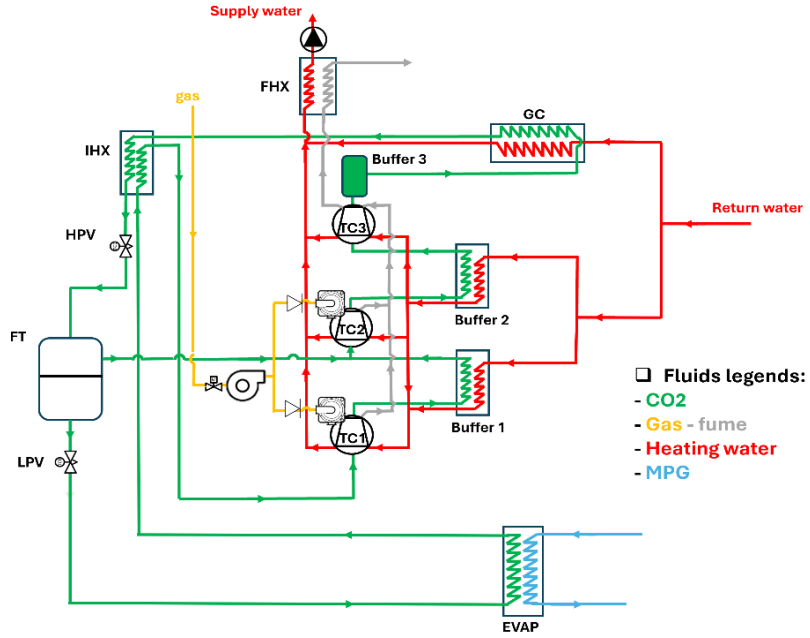

Figure 1: Schematic representation of the TCHP cycle.

3 DYNAMIC MODEL

This section outlines the modeling approach for the components of a TCHP. The models are implemented in Python, utilizing the CoolProp library to compute the thermophysical properties of CO_2 developed by Bell et al. (2014). In conventional electric driven VCC, the expansion valve and compressor are assumed steady, as their dynamics are faster compared to the ones of the heat exchangers. The use of a TC instead of a conventional compressor changes this rule. In fact, the slowest dynamic in a TCHP cycle corresponds to the TCs due to the high inertia of their heaters, which also causes the slow changes of the refrigerant characteristics (mass flow rate, temperature and pressure). Since we can't represent TC dynamically as it largely exhausts the computation cost, we consider that the heater temperature is an input rather than burner fan speed, this allows us to safely represent the TC with steady state regression models. The dynamic variations of the EEVs are significantly faster than those of the heat exchangers. Consequently, the EEVs and TCs are modeled statically using algebraic equations, while the dynamic behavior of the heat exchangers and flash tank is captured through differential equations. The developed dynamic model respects the following assumptions: (1) No pressure drop is considered on either side of the fluid, (2) Mass variation is only accounted for in the last control volume of a heat exchanger, (3) Heat conduction fluxes are neglected, and (4) The secondary fluids are assumed to be incompressible.

3.1 Heat Exchangers

Other than the two main heat exchangers (GC and EVAP), the cycle contains several heat exchangers that recover heat from within the cycle. The GC and EVAP are made of brazed plate heat exchangers constructed from copper, specifically designed to handle the high-pressure levels of CO_2 (see Table 1). Both heat exchangers are spatially discretized into N_{gc} and N_{evap} control volumes respectively (Figure 2). According to the continuity principle for CO_2, the derivative of density with time can be expressed as:

$$\left(\left(\frac{\partial \rho}{\partial h}\right)_p \frac{\partial h}{\partial t} + \left(\frac{\partial \rho}{\partial p}\right)_h \frac{\partial p}{\partial t}\right)_i = \frac{1}{V_i}\left(\dot{m}_{j-1} - \dot{m}_j\right) \quad (1)$$

From the energy balance equation:

$$\left(\rho\frac{\partial h}{\partial t}-\frac{\partial p}{\partial t}\right)_i = \frac{1}{V_i}\left(\dot{Q}_{f,i} + \dot{m}_{j-1}\left(h_{j-1}-h_i\right)-\dot{m}_j\left(h_j-h_i\right)\right) \quad (2)$$

In the IHX, eq. (2) is used to express both sides of fluids as they are both CO_2. While in the remaining heat exchangers, where water or MPG is the secondary fluid, the temperature variation is described by the energy balance equation:

$$\left(mc\frac{\partial T}{\partial t}\right)_{sf,i} = \dot{Q}_{sf,i} + \dot{m}_{sf,j}h_{sf,j} - \dot{m}_{sf,j-1}h_{sf,j-1} \quad (3)$$

Then the temperature variation of the wall is described as a function of the heat convection with CO_2 and secondary fluid:

$$\left(mc\frac{\partial T}{\partial t}\right)_{wall,i} = -(\dot{Q}_{f,i} + \dot{Q}_{sf,i}) \quad (4)$$

Table 1: Design parameters of the GC and EVAP.

	Model	Number of plates	Total Volume [l]	Max working temperature [°C]	Max working pressure [bar]	Total Area [m2]
GC	C042	56	1.65	200	140/30	1.0422
EVAP	C096	28	1.917	200	100/30	1.235

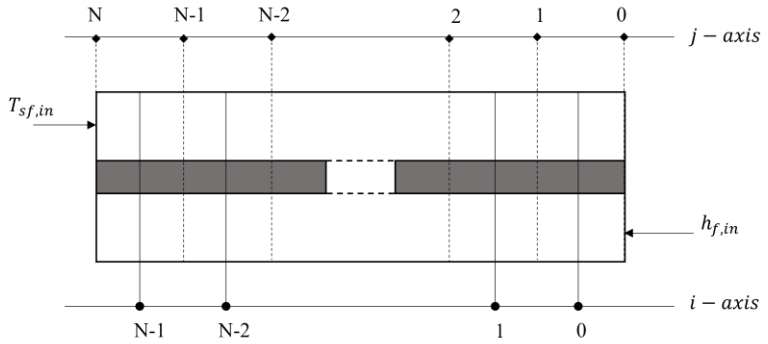

Figure 2: Spatial discretization of a heat exchanger.

Where the heat exchange rates on the working fluid and secondary fluid side are as follows:

$$\dot{Q}_{f,i} = U_{f,i}A_i\left(T_{wall,i}-T_{f,i}\right) \quad (5)$$

$$\dot{Q}_{sf,i} = U_{sf,i}A_i\left(T_{wall,i}-T_{sf,i}\right) \quad (6)$$

The wall definition of the heat transfer coefficient is necessary to catch the heat transfer between CO_2 and secondary fluid. This coefficient might be affected by the phase of CO_2 fluid, as well as whether it's being cooled or heated. Several works have been done to find the suitable heat transfer coefficient for CO_2 according to its phase, concluding that no correlation can be reliably generalized till now. For this reason, we derive our own correlations in the evaporator and the gas cooler by tuning the Dittus–Boelter's with real data. The Nusselt number correlation according to the CO_2 phase is as follows:

- In supercritical region ($p > 73.8\ bar$):

$$Nu = 0.005Re^{0.9}\mathrm{Pr}^{0.18} \quad (7)$$

- In subcritical region ($p < 73.8\ bar$) and two-phase ($0 < X < 1$):

$$Nu = 0.1Re^{0.8}\mathrm{Pr}^{0.6}X^{0.2} \tag{8}$$

In single phase, Dittus–Boelter's correlation is used without modification:

$$Nu = 0.023Re^{0.8}\mathrm{Pr}^{0.4} \tag{9}$$

For simulations, the number of control volumes considered for the EVAP and GC are 12 and 8, respectively. Meanwhile, the other heat exchangers including buffer 1, buffer 2, IHX, RHX, and the FT each consist of 1 control volume. A detailed modeling approach for a FT was outlined by Qiao et al. (2015). The coolers, which are major heat recovery exchangers in a TCHP, are estimated with regression models, as will be detailed in the upcoming sections.

3.2 Expansion Valves

The cycle involves two electronic expansion valves (LPV and HPV). The LPV is used to control the superheat by manipulating the opening of the valve OP_{LPV}, while the HPV is used to regulate the high pressure by also manipulating the valve opening OP_{HPV}. Assuming the expansion to be an isenthalpic process, the mass flow rates through the LPV and HPV can be represented as follows, respectively:

$$\dot{m}_{LPV} = 3.13 \times 10^{-9}\ OP_{LPV}\sqrt{\rho_{ft,l}\left(p_{ft} - p_{evap}\right)} \tag{10}$$

$$\dot{m}_{HPV} = 5.77 \times 10^{-9} OP_{HPV}\sqrt{\rho_{gc}\left(p_{gc} - p_{ft}\right)} \tag{11}$$

Tuning of eqs. (10) and (11) is done using steady state data that was previously used by Fallahsohi (2023).

3.3 Thermal Compressors, Coolers, and Fume Heat Recovery:

The thermal compressor (TC) exhibits the slowest dynamics in the system due to the high thermal inertia of its heater. Consequently, heater temperatures are treated as independent variables within regression models, embedding the slow dynamics into the derived correlations. Step tests on the third motor speed (ω_3) revealed a negligible impact on system variables, leading to its exclusion from the model. The temperature of the third heater, for which direct measurements are unavailable, is combined with that of the second heater to prevent model stiffness arising from the coupling of algebraic mass flow equations and differential pressure equations. The inlet temperature is also excluded to due low relevancy on outputs compared to other inputs (Salame et al. (2024a)) .The regression models represent the mass flow rate entering the GC, denoted as $\dot{m}_{TC23}$, the discharge temperature or the temperature of CO_2 entering the GC, denoted as $T_{gc,in}$ and the resulting heat recovered by the second and third TCs, denoted as $\dot{Q}_{cooler23}$, all defined as follows:

$$LR_{23,i}\left(R_{p23}, R_{T2}, \omega_2\right) \quad i \in \{1,2,3\} \tag{12}$$

LR_i are linear regression model types. R_{p23} is the pressure ratio between GC and FT and R_{T2} is the temperature ratio between heater 2 and inlet water both in Kelvin. We chose not to complicate the models due to the limited number of samples and to avoid overfitting. The first TC's derived regression models represent the mass flow rate leaving the EVAP, denoted as $\dot{m}_{TC1}$, the discharge temperature, and the heat recovered by the first cooler, denoted as $\dot{Q}_{cooler1}$:

$$LR_{1,i}\left(R_{p1}, R_{T1}, \omega_1\right)\ i \in \{1,2,3\} \tag{13}$$

R_{p1} is the pressure ratio between FT and EVAP and R_{T1} is the temperature ratio between heater 1 and inlet water.

3.4 Performance Metric for A TCHP:

In an electrically driven heat pump, the COP is defined as the ratio between the total recovered heat over the electric consumption by the motor. In our work, the compressors run by heat as a primary energy source and electricity as secondary. With a small contribution of electricity compared to heat, we evaluate our TCHP with a thermal COP, defined as the ratio between total heat rate recovered $\dot{Q}_{heat,tot}$ over total heat rate consumed $\dot{Q}_{comb}$ (combustion power):

$$COP = \frac{\dot{Q}_{heat,tot}}{\dot{Q}_{comb}} \tag{14}$$

The total heat rate recovered is distributed as follows:

$$\dot{Q}_{heat,tot} = \dot{Q}_{gc} + \dot{Q}_{cooler1} + \dot{Q}_{cooler23} + \dot{Q}_{fhx} + \dot{Q}_{buffer1,2} \tag{15}$$

And the combustion power is:

$$\dot{Q}_{comb} = \dot{m}_{CH4} LHV \tag{16}$$

Where $\dot{m}_{CH4}$ is the methane gas mass flow rate which is regulated by the burner fan speed and LHV is its lower heating value.

By taking the model assumptions into consideration, equations (1)-(4) results in the following state vector (Figure 3):

$$x = [p_{gc}, \bar{h}_{gc}, \bar{T}_{gc,wall}, p_{evap}, \bar{h}_{evap}, \bar{T}_{evap,wall}, p_{buff1}, h_{buff1}, T_{buff1,wall}, h_{buff2}, T_{buff2,wall}, h_{ihx1}, h_{ihx2}, T_{ihx,wall}, p_{ft}, h_{ft}] \tag{17}$$

And the input vector containing all the inputs of the cycle:

$$u = [OP_{HPV}, OP_{LPV}, T_{heater1}, T_{heater2}, \omega_1, \omega_2, T_{w,in}, \dot{m}_w, T_{mpg,in}, \dot{m}_{mpg}] \tag{18}$$

Where $\bar{h}_{evap,wall}$ and $\bar{T}_{evap,wall}$ are vectors of order N_{evap} and $\bar{h}_{gc,wall}$ and $\bar{T}_{gc,wall}$ are vectors of order N_{gc}. The resulting model is a system of ODEs:

$$\dot{x} = f(x, u) \tag{19}$$

Which is to be solved and simulated in the next section. The resulting simulations are used to validate the model predicted high and low pressures of CO_2, outlet water and mpg temperatures, the resulting total heating power and COP with experimental data.

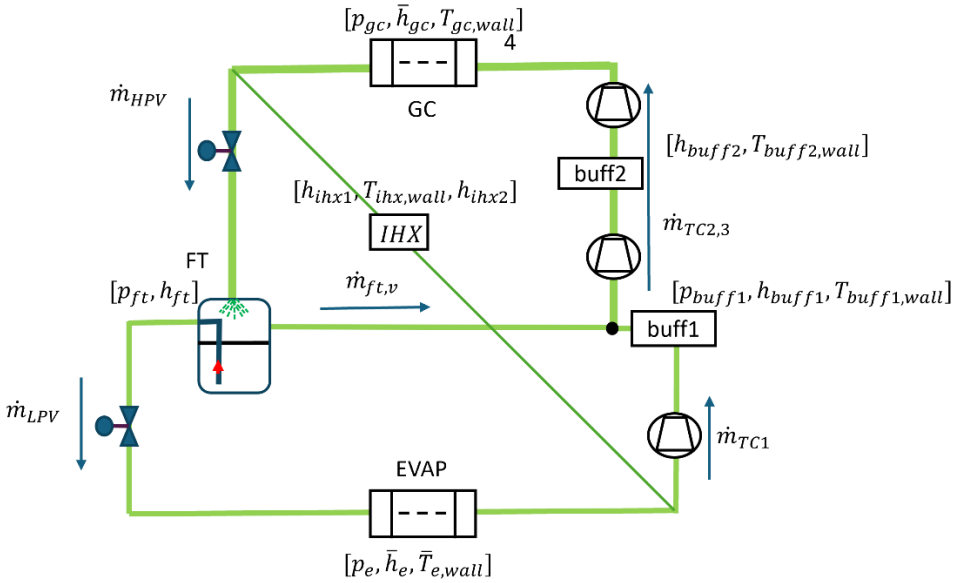

Figure 3: Model vectors represented on the cycle.

4 RESULTS AND DISCUSSIONS

The validation of the model is conducted in two phases: steady state and dynamic. The steady state data, consisting of 15 points under various operating conditions, were collected using several distributed sensors throughout the cycle. This steady state data was utilized to fine-tune our empirical static correlations for the EEVs and TCs. The dynamic data was collected from the commercialized machine, so we had fewer measured variables. We choose to validate the model with three main inputs, that are the high- and low-pressure valves openings and burner fan speed.

4.1 Steady State

The initialization of state vector (equation (17)) is very important for the solving of (19). At the start of each steady-state simulation, the initial pressure values are intentionally set with a 5 bar offset from the expected steady-state values to ensure proper model stabilization. The CO_2 enthalpies are initialized with the corresponding inlet enthalpies, and the wall temperatures are set equal to the temperatures of the secondary fluid to reflect realistic boundary conditions. Each simulation runs for 600 seconds, with final predictions obtained by averaging the results over the last 10 seconds to ensure that a steady state has been reached. The third-order Runge-Kutta method is chosen as the solver due to its reliability in handling stiff ordinary differential equations. According to Figures 4 and 5, the resulting mean absolute percentage error (MAPE) for the evaporator and gas cooler pressure values are 5.6% and 2.2% respectively. The mean absolute error (MAE) of the outlet temperatures of the evaporator and gas cooler are 3.6 K and 1.7 K respectively. The resulting COP values of the TCHP are predicted with a MAPE of 5.7% (Figure 6).

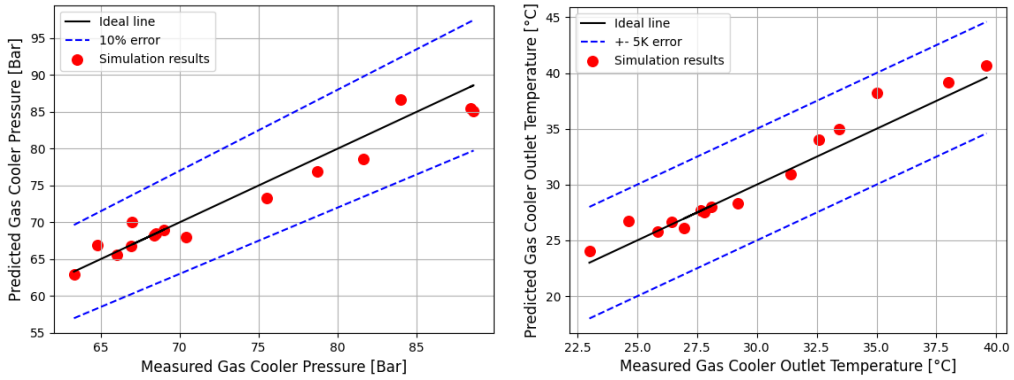

Figure 4: Steady state parity plots showing the gas cooler (a) pressure and (b) outlet temperature.

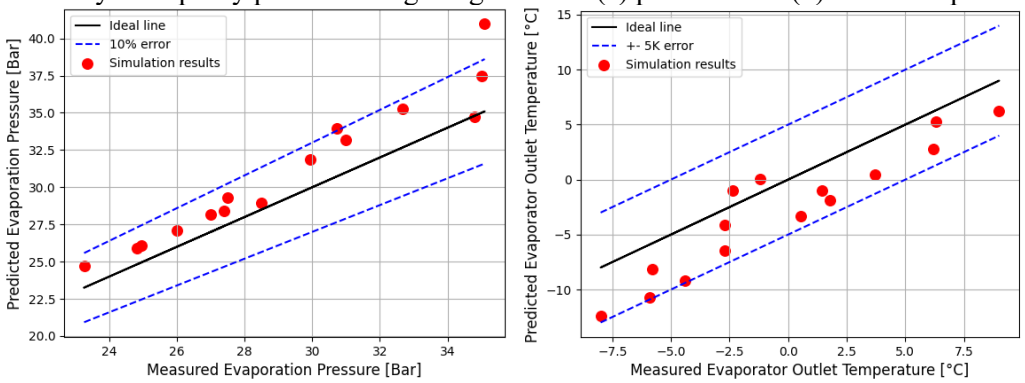

Figure 5: Steady state parity plots showing the evaporator (a) pressure and (b) outlet temperature.

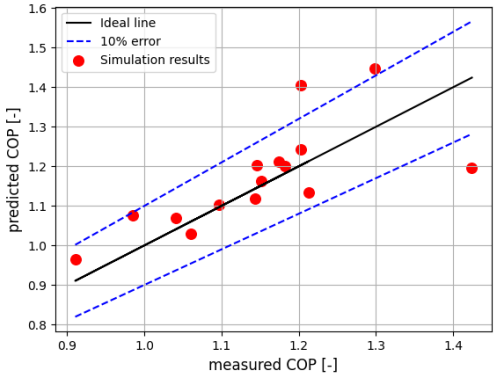

Figure 6: Steady state parity plots showing the thermal COP of the TCHP.

4.2 Dynamic Validation

The dynamic data was collected from the commercialized TCHP system, so fewer sensors were used due to practical constraints of the setup. The data was obtained through pseudo random binary sequence (PRBS)-like tests on the HPV and LPV openings and step changes on burner fan speed. The validated variables (which correspond to the available measurements) include the GC and EVAP pressures and outlet temperatures, as well as the outlet water and MPG temperatures. These measurements are used to calculate the total heating output power of the cycle, the evaporation heat exchange rate, and the COP. While one of the inputs changes, the others remain constant (Table 2):

Table 2: Constant inputs during tests.

Inputs	Values [units]
ω_1, ω_2	150 [rpm]
ω_b	4411 [rpm]
OP_{HPV}, OP_{LPV}	50 [%]
$T_{heater1}, T_{heater2}$	662, 610 [°C]
$T_{w,in}, T_{mpg,in}$	28, 6 [°C]
$\dot{m}_w, \dot{m}_{mpg}$	0.23, 0.275 [kg/s]

Figure 7 shows the variation of outputs measurements when the HPV opening is varied in a PRBS fashion. The largest influence is observed on the high pressure, where the model exhibits transient behavior compatible with the data, as well as good convergence to steady-state values, due to HPV's role in pressure regulation, while EVAP heat exchange rate and pressure are slightly affected. The resulting heating power and COP are also well captured by the model. Figure 8 illustrates the output variations when the LPV opening is varied in a PRBS manner. The greatest influence is observed on the low pressure due to its strong correlation with mass flow rate changes driven by LPV, while less negligible influence is seen on the other outputs. Figure 9 shows several step changes that were applied to the burner fan speeds on a time range of 260 minutes because of the slow variation of the heater

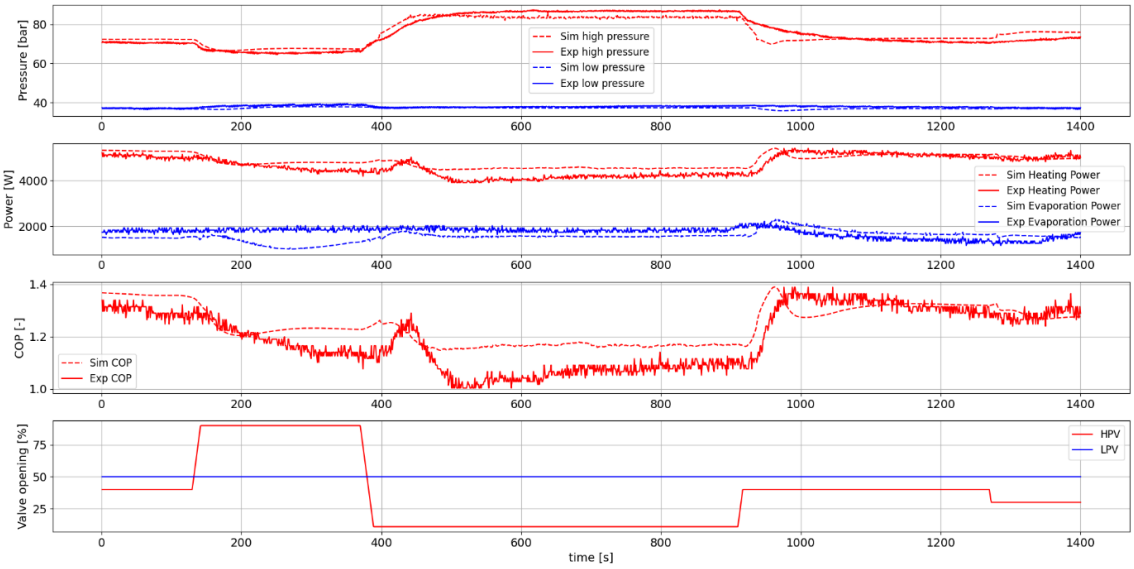

Figure 7: Dynamic model validation of high-pressure variation with a PRBS test.

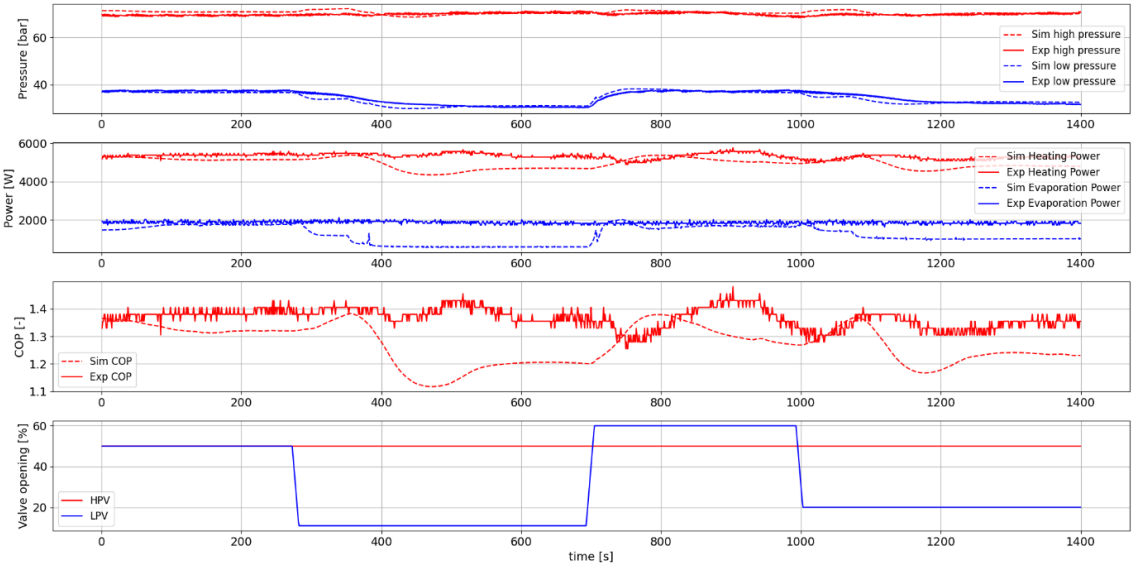

Figure 8: Validation of superheat predictions based on a PRBS test on the LPV.

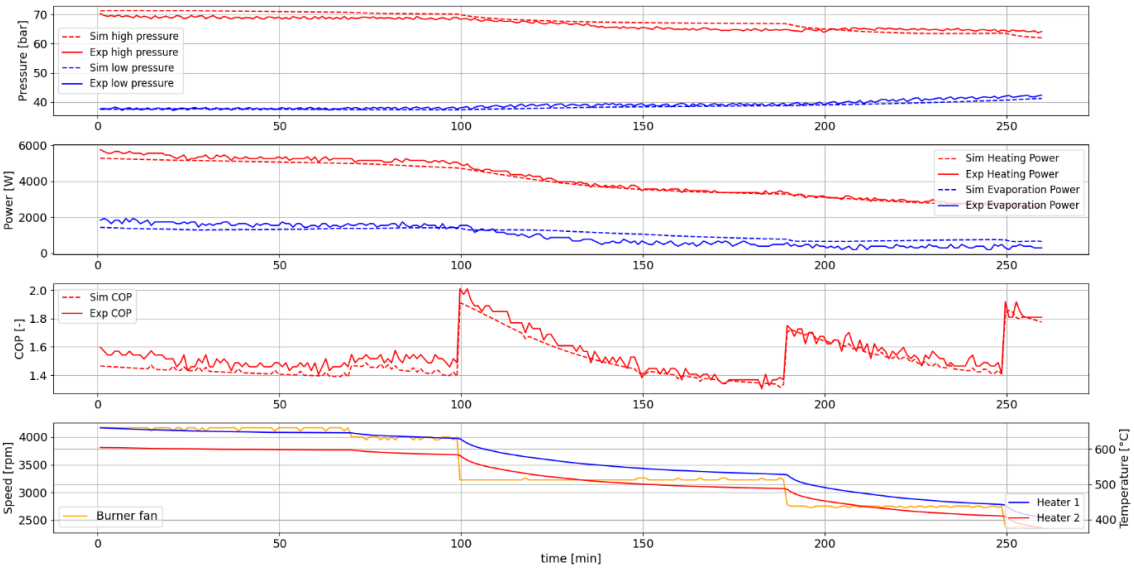

Figure 9: Model validation with step tests on the burner fan speed.

temperature. The burner fan speed variations (also heater 1 and 2 temperatures) are directly affecting the EVAP and GC, which justifies the variations on all the outputs that were also well captured by our model. The resulting MAPE (or MAE) and R^2 of the predictions at each test are summarized in Table 3. An R^2 value of 1 corresponds to a perfect fit. The resulting MAPEs of the pressures, output heating power, and COP are less than 7 %. The MAE for outlet water and mpg temperatures are less thank 1 °C. The negative fits observed for LPV on GC outputs and for HPV on EVAP outputs are mainly due to the lack of direct influence of these inputs on the respective components—LPV has minimal effect on the GC, and HPV has limited impact on the EVAP—combined with relatively flat, noise-affected output signals that make the model less effective than a simple average in these cases. Burner fan (BF in Table 3) shows acceptable fit on all outputs, due its direct effect on them. From the fit evaluation (R^2 values), we can deduce that HPV and BF have a great influence on the performance and thus are very important to control, as their regulation can optimize key outputs. We can reliably say that the effect on the TCHP performance of HPV and BF is well captured and can be used for control development. Based on these results, the model is validated and can be considered reliable for future control and optimization approaches, as it effectively predicts the dominant dynamics.

Table 3: The $MAPE$ and R^2 of the model outputs predictions at different carried step tests on the LPV, HP, and burner fan speed.

	MAPE [%] or **MAE** [°C]			R^2 [-]		
Tests	**HPV**	**LPV**	**BF**	**HPV**	**LPV**	**BF**
$\boldsymbol{p_c}$	3.2	1.57	2.36	0.87	-4.6	0.24
$\boldsymbol{p_e}$	2	2.26	1.67	-1.6	0.87	0.65
$\boldsymbol{T_{w,out}}$ (MAE)	0.39	0.33	0.16	0.6	-9.96	0.95
$\boldsymbol{T_{mpg,out}}$ (MAE)	0.53	0.77	0.37	0.35	0.54	0.74
$\boldsymbol{\dot{Q}_{heat,tot}/COP}$	5.7	7	3.27	0.52	-10	0.97

5 Conclusion

In this work, we introduced a dynamic model for a multi-stage CO_2 thermal compressor heat pump technology driven by heat. The finite volume method was used to discretize the gas cooler and evaporator in space, while the remaining heat exchangers and flash tank were treated as single control volumes. Mass and energy balance equations were applied to each component, and the system was connected through thermal compressors and expansion valves, which were statically modeled. A steady-state dataset of 15 samples and dynamic data from several step tests on key inputs were used to validate the derived model. Statically, the MAPE of the predicted COP, high-pressure, and low-pressure values are 5.7 %, 5.6 %, 2.2 %. While the MAE of the outlet temperatures of gas cooler and evaporator are 1.7 K and 3.6 K. Dynamically, through step tests on key inputs, the model was able to accurately capture the transient responses of the outputs. Therefore, the model can be used as a reference for future control and optimization applications.

NOMENCLATURE

X	Vapor quality	(-)	**Abbreviations**	
T	Temperature	(°C)	PRBS	Pseudo random binary sequence
p	Pressure	(bar)	CO_2	Carbon dioxide
m	Mass	(Kg)	EVAP	Evaporator
h	Enthalpy	(Kg/J)	GC	Gas cooler
V	Volume	(m^3)	IHX	Internal heat exchanger

$\dot{m}$	Mass flow rate	(Kg/s)	RHX	Recover heat exchanger
R_T	Temperature ratio	(-)	FT	Flash tank
R_p	Pressure ratio	(-)	LPV	Low pressure valve
Pr	Prandtl number	(m^2/s)	HPV	High pressure valve
Nu	Nusselt number	(-)	MAPE	Mean absolute percentage error
OP	Valve opening	(%)	TC	Thermal compressor
A	Area	(m^2)	TCHP	Thermal compressor heat pump
U	Convective coefficient	(W/K. m^2)	COP	Coefficient of performance
Re	Reynolds number	(-)	ODE	Ordinary differential equation
$\dot{Q}$	Heat exchange rate	(W)	FV	Finite Volume
ω	Speed	(rpm)	MB	Moving boundary
Subscripts			MAE	Mean absolute error
f	Working fluid		MAPE	Mean absolute percentage error
sf	Secondary fluid		R^2	Coefficient of determination
w	Water			
mpg	Glycol mixture			
l	Liquid			
v	Vapor			

REFERENCES

Bell, I.H., Wronski, J., Quoilin, S., Lemort, V., (2014). Pure and Pseudo-pure Fluid Thermophysical Property. Evaluation and the Open-Source Thermophysical Property Library CoolProp, *Ind. Eng. Chem. Res.,* 53(6), p. 2498-2508.

Bendapudi, S., Braun, J.E., and Groll, E.A., (2008). A comparison of moving-boundary and finite-volume formulations for transients in centrifugal chillers. International Journal of Refrigeration 31(8):1437–52.

Diniz, H. A. G., Paulino, T. F., Pabon, J. J. G., Maia, A. A. T., and Oliveira, R. N. (2021). Dynamic model of a transcritical CO_2 heat pump for residential water heating. Sustain-ability, 13(6).

Fallahsohi, H. (2023). Energy analysis of the heat pump operating with supercritical CO_2 driven by thermal compression. American Journal of Engineering Research, 12(11), p. 61-74

He, X.D., Liu, S., and Asada, H., (1997). Modeling of vapor compression cycles for multivariable feedback control of HVAC systems. ASME Journal of Dynamic Systems Measurement & Control 119(2):183–91.

Ibsaine, R., Joffroy, J.M., Stouffs, P., (2016). Modelling of a new thermal compressor for supercritical CO_2 heat pump, *Energy*, Volume 117, Part 2, p. 530-539.

IEA (2024), *World Energy Outlook 2024*, IEA, Paris https://www.iea.org/reports/world-energy-outlook-2024, Licence: CC BY 4.0 (report); CC BY NC SA 4.0 (Annex A)

Ko, J., Takata, N., Thu, K., and Miyazaki, T. (2020). Dynamic modeling and validation of a carbon dioxide heat pump system. Evergreen, 7(2):172–194. P2020.

McKinley, T.L., Alleyne, A.G., (2008). An advanced nonlinear switched heat exchanger model for vapor compression cycles using the moving-boundary method, *International Journal of Refrigeration*, Volume 31, Issue 7, Pages 1253-1264, ISSN 0140-7007.

Neksa, P., 2002. CO_2 heat pump systems, *Int J Refrig* 25, p. 421–427.

Peralez, J., Nadri, M., Dufour, P., Tona, P., Sciarretta, A., (2017). Organic Rankine Cycle for Vehicles: Control Design and Experimental Results. IEEE Transactions on Control Systems Technology, 25 (3), pp.952 - 965.

Pfafferott, T., Schmitz, G., (2004). Modelling and transient simulation of CO_2-refrigeration systems

with Modelica, *International Journal of Refrigeration*, Volume 27, Issue 1, Pages 42-52, ISSN 0140-7007.

Qiao, H., Xu, X., Aute, V., Radermacher, R., (2015). Transient modeling of a flash tank vapor injection heat pump system – Part I: Model development, *International Journal of Refrigeration*, Volume 49, Pages 169-182, ISSN 0140-7007.

Rasmussen, B.P. (2005). Dynamic Modeling and Advanced Control of Air Conditioning and Refrigeration Systems. Ph.D. Thesis, University of Illinois, Urbana, IL.

Rasmussen, B.P., (2012). Dynamic modeling of vapor compression systems—Part I: Literature review. Science and Technology for the Built Environment 18(5):934–55.

Salame, A., Lemort, V., Dufour, P., and Nadri, M., (2024a). An Empirical Model for a CO_2 Thermal Compressor Based on Experimental Data. *International Compressor Engineering Conference*. Paper 2868.

Salame, A., Lemort, V., Dufour, P., Nadri, M., and Ibsaine, R., (2024b). Dynamic Modelling Approach of a Thermal Compressor and Validation Based on Experimental Tests. ECOS24 conference proveedings, paper 193.

Sarkar, J., Bhattacharyya, S., Gopal, M.R., 2004. Optimization of a transcritical CO_2 heat pump cycle for simultaneous cooling and heating applications, *International Journal of Refrigeration*,Volume 27, Issue 8, Pages 830-838, ISSN 0140-7007.

Yang, J.L., Ma, Y.T., Li, M.X., Hua, J., (2010). Modeling and simulating the transcritical CO_2 heat pump system, *Energy*, Volume 35, Issue 12, Pages 4812-4818, ISSN 0360-5442.

Zheng, L., Deng, J., He, Y., and Jiang, P. (2015). Dynamic model of a transcritical CO_2 ejector expansion refrigeration system. International Journal of Refrigeration, 60:247–260.

ACKNOWLEDGEMENT

The French ministry of higher education and research is acknowledged for the financial support of this CIFRE PhD thesis 2022-0549.